Observation of wave-induced chaotic radial transport in a laboratory terrella experiment*

H. P. Warren,[†,a)] M. E. Mauel, D. Brennan, and S. Taromina
Department of Applied Physics, Columbia University, New York, New York 10027

(Received 8 November 1995; accepted 4 January 1996)

The wave-induced chaotic radial transport of energetic electrons has been observed in a laboratory terrella, the Collisionless Terrella Experiment (CTX) [H. P. Warren and M. E. Mauel, Phys. Plasmas **2**, 4185 (1995)]. In the experiment electron-cyclotron-resonance heating (ECRH) is used to create a localized population of trapped energetic electrons which excite drift-resonant electrostatic fluctuations. Measurements with multiple high-impedance floating potential probes are used to determine the amplitude, frequency, and mode structure of the observed fluctuations. Energetic electron transport is observed with gridded particle detectors. Poincaré surfaces of section indicate that increases in the flux of energetic electrons to the detectors occur only when fluctuations which meet the conditions for global chaos are present. Quasilinear transport simulations do not reproduce several important features of the experimental measurements. In contrast, Hamiltonian simulations reproduce many of the salient temporal characteristics of the experimental measurements and indicate that the persistence of phase-space correlations plays an important role in the energetic electron transport observed in the experiment. © *1996 American Institute of Physics.* [S1070-664X(96)91405-X]

I. INTRODUCTION

Understanding the transport of energetic particles is a fundamental problem of laboratory, astrophysical, and space plasmas. Of particular interest is transport in collisionless plasmas driven by non-linear wave-particle resonances. For example, chaotic radial transport which preserves the first two adiabatic invariants μ and J but breaks ψ is an essential mechanism for both the injection of particles into the Earth's magnetosphere and their acceleration.[1] This transport is driven by sudden, large-scale perturbations in the Earth's geomagnetic and convection electric fields caused by variations in the solar wind and interplanetary magnetic field.[2]

Previously we reported the first observation of wave-induced chaotic radial transport in a laboratory terrella experiment, the Collisionless Terrella Experiment (CTX).[3,4] One of the primary goals of CTX is to study the process of chaotic radial transport in dipole magnetic fields which preserves the first two adiabatic invariants μ and J.[5] In particular, these experiments investigate the relationship between fluctuation spectra and models of energetic particle transport and provide the first laboratory tests of Hamiltonian methods which can be used to simulate transport in collisionless plasmas.

In the experiment electron-cyclotron-resonance heating (ECRH) is used to create a highly localized population of magnetically trapped energetic electrons.[6] While the ECRH is on, the energetic electrons excite quasiperiodic bursts of electrostatic fluctuations which resonate with the precessional drift motion of the trapped particles. Drift-resonant electrostatic waves are also observed during the afterglow of the plasma discharge, when the ECRH has been turned off. During both times, the observed fluctuations have a complicated time-dependent frequency content.

By computing Poincaré surfaces of section we find that during the instability bursts the measured spectral characteristics of the drift-resonant fluctuations meet the conditions required for global chaotic particle transport. Coincident with the instability bursts, energetic electron transport is observed with gridded particle detectors located outside the hot electron ring. The observed transport is strongly modulated at frequencies related to the precessional drift-frequency of the energetic electrons. During the afterglow, Poincaré surfaces of section indicate that the instability wave spectrum does not satisfy the conditions for global chaos and no enhanced transport is observed experimentally.

The Poincaré surfaces of section which model particle motion during the instability bursts show that phase space is strongly chaotic and suggest that quasilinear theory should be applicable. However, in order to model the spatial and temporal evolution of particle fluxes observed in the experiment, simulations using the guiding center drift Hamiltonian are necessary. One such simulation involves computing the flux of equatorial particle trajectories to a small region of phase space which represents the particle detector. This simulation reproduces the modulation depth and frequency of the experimentally observed electron flux. When the results of the Hamiltonian transport simulation are compared with a simple quasilinear transport model we find that the predictions of the quasilinear model do not reproduce the experimentally observed modulations and underestimate the maximum particle fluxes measured in the experiment.

II. THE COLLISIONLESS TERRELLA EXPERIMENT

The CTX experimental device consists of a dipole electromagnet suspended mechanically in an axisymmetric aluminum vacuum vessel 1.4 m in diameter. The magnet is sup-

*Paper 2IA1, Bull. Am. Phys. Soc. **40**, 1666 (1995).
†Invited speaker.
a)Present address: Naval Research Laboratory, Washington, DC 20375.

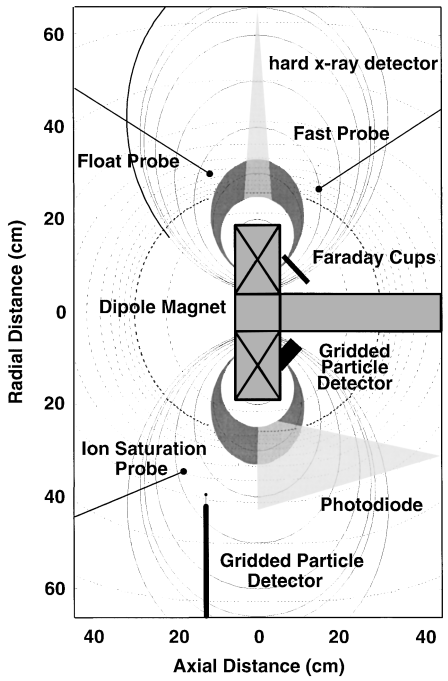

FIG. 1. The magnetic field geometry of CTX. The solid lines represent magnetic field lines and the dotted lines represent surfaces of constant magnetic field. The location of several plasma diagnostics and the approximate location of the hot electron ring are also shown.

ported by a stainless steel casing which houses the electrical and cooling leads. The strength of the dipole magnetic field is approximately 15 kG at the face of the magnet and falls off to less than 50 G at the wall. The magnetic field lines and mod-B surfaces of the dipole magnet used in CTX and are shown in Fig. 1.

A pulse of microwaves lasting approximately 0.5 s is used to break down and heat hydrogen gas which is puffed into the vacuum chamber both at the beginning and during a discharge. The microwave source is a continuous wave magnetron which has a peak output of 1.5 kW at a frequency of 2.45 GHz. The electron gyrofrequency equals the frequency of the applied microwaves along the surface defined by $B_0 \equiv B \simeq 875$ G. The equatorial field strength of the dipole magnet has this value at a radial distance of $R_0 \equiv R \simeq 27$ cm and this defines the center of the hot electron ring or artificial radiation belt.

Plasma diagnostics include a series of Langmuir and high impedance floating potential probes situated at five locations throughout the vacuum vessel. The probes can be repositioned radially to examine the density and potential fluctuations at different flux surfaces. Multiple probe measurements allow the direction of propagation, the azimuthal mode number and radial mode structure of the observed fluctuations to be determined.

A krypton proportional counter is positioned at the midplane of the magnetic field and is used to measure hard x-ray emission at energies between 1–60 keV. The counter is collimated to view the equatorial region of the dipole magnetic field. X-ray spectra are collected and stored at 50 ms intervals during the plasma discharge.

Gridded particle detectors are located inside the vacuum chamber both near the equatorial midplane and in the polar region. The equatorial particle detector is supported by a metal rod which extends from the vacuum chamber wall and can be repositioned to measure particle flux at different radial positions. There are five polar particle detectors which are situated so that the magnetic field at each detector is the same. The gridded particle detectors are biased to repel ions and electrons with energies less than 100 eV.

Five Faraday cups are also located in the polar region of the dipole magnetic field. The Faraday cups are situated to view the same field lines as the polar gridded particle detectors but rotated 90° in azimuthal angle. The Faraday cups are biased to repel ions.

Three photodiodes are positioned to measure radiation emitted from the plasma at wavelengths from 400–1100 nm. The photodiodes can be collimated to look at the inside of the hot electron ring ($R<27$ cm), the center of plasma (27 cm$<R<54$ cm), and the outside of the plasma ($R>54$ cm).

III. EXPERIMENTAL OBSERVATIONS

The intensity of the hot electron population is characterized by the hard x-ray emission produced by electron-ion and electron-neutral bremsstrahlung. A fraction of these x-rays are detected with the krypton proportional counter. The observed distributions are non-Maxwellian, characteristic of microwave-heated electrons.[7] The electrons with energies between 1–10 keV are referred to as the ''warm'' population, and electrons with energies above 10 keV are referred to as the ''hot'' population. When the microwave power is switched off, the ''hot'' population persists for 5–20 ms, defining the discharge ''afterglow.''

When an intense hot electron population is produced, drift-resonant fluctuations ($\omega \sim \omega_{dh}$) are observed both while the ECR heating is on and in the afterglow. During the heating, the fluctuations occur in quasiperiodic bursts lasting approximately 300–500 μs. During the afterglow, the drift-resonant oscillations persist for as long as several milliseconds. At both times, the observed instabilities propagate azimuthally in the direction of the electron ∇B drift, are flute-like with a constant phase along a field-line, and have a broad radial structure extending throughout the plasma. The saturated amplitudes of the floating potential oscillations present at both times are similar, typically 100–200 V.

Fourier analysis indicates that the quasiperiodic bursts consist of incoherent, broad-band fluctuations with frequencies typically below 2 MHz, although some particularly intense bursts have frequencies as high as 5 MHz. The instabilities observed during the afterglow are more coherent than those observed during the ECRH and have a higher range of frequencies, $f \sim$ 1–12 MHz.

The fluctuations observed during the ECRH also differ from those observed in the afterglow in terms of their azimuthal mode number. During the quasiperiodic instability bursts, the azimuthal mode number is usually limited to $m=1$, except in the most intense bursts when some high-frequency, $m=2$ modes are observed. In the afterglow,

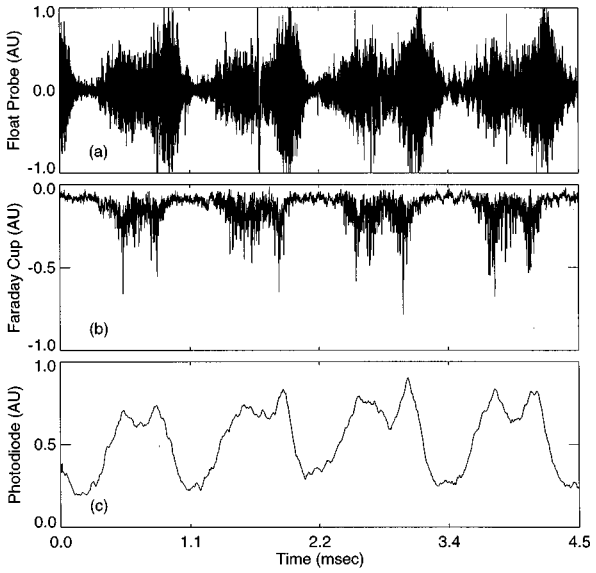

FIG. 2. Simultaneous measurements of drift-resonant fluctuations and energetic electron transport during the microwave heating. (a) Floating potential oscillations illustrate intense, quasiperiodic bursts correlated with (b) rapid increase of electron flux to the Faraday cup and (c) visible photon emission from the plasma measured by the center photodiode.

$m \leqslant 6$, and there are often multiple waves with the same azimuthal mode number present simultaneously.

The drift-resonant fluctuations observed in the experiment are related to the hot electron interchange instability that has been observed in other ECR heated magnetic mirror experiments.[8,9] The linear theory of the hot electron interchange, assuming slab geometry and a monoenergetic distribution of electrons, was developed by Krall[10] for $\omega \ll \omega_{ci}$ and by Berk[11] for $\omega \sim \omega_{ci}$ and the characteristics of the observed fluctuations are generally similar to those predicted by these simple theories.

Coincident with the bursts of wave activity observed during the ECRH are increases in the flux of energetic electrons to the equatorial gridded particle detector and the polar gridded particle detectors. As shown in Fig. 2, the radiation detected by the center photodiode also rises significantly during the instability bursts and is diminished between them. This last fact is particularly interesting. Recall that the use of microwave heating leads to a highly localized plasma. Beyond the hot electron ring the density of neutral hydrogen should increase rapidly. As the drift-resonant fluctuations drive energetic electrons out radially, they can ionize the surrounding neutral gas. Also recall that μ and J conserving radial transport leads to an adiabatic decompression with particle energy decreasing as $\sim 1/R^3$. This increases the Coulomb cross section and makes both electron-neutral and electron-ion collisions more frequent.

The characteristics of the transport measurements suggest a definite relationship between the spectral content of the waves and the observed energetic particle flux. The level of the electron flux is not simply related to the amplitude of the fluctuations but depends on the spectral content of the wave. Also note that the energetic electron flux observed both with the equatorial gridded particle detector and the Faraday cups is strongly modulated at frequencies related to the precessional drift-frequency electrons. The connection between the spectral content of the fluctuations and the electron flux will be examined in detail in the next section.

IV. WAVE-INDUCED PARTICLE TRANSPORT

The interaction of energetic electrons with the drift-resonant electrostatic waves observed in the experiment can be described by the guiding center drift Hamiltonian[12]:

$$\mathscr{H} = \frac{m_e c}{2e}\rho_{\|}^2 B^2 + \mu\frac{cB}{e} - c\Phi, \tag{1}$$

where m_e and e are the electron mass and charge, c is the speed of light, B is the magnitude of the dipole magnetic field, $\mu \equiv m v_{\perp}^2/2B$ is the magnetic moment, $\rho_{\|} \equiv v_{\|}/B$, and Φ is the electrostatic potential. For a curl-free magnetic field, the canonical coordinates of the guiding center drift Hamiltonian, $(\rho_{\|}, \chi)$, and (ψ, φ), are essentially the magnetic coordinates defined by: $\mathbf{B} = \nabla\psi \times \nabla\varphi = \nabla\chi$. The function $\psi = M \sin^2\theta/R$ is proportional to the magnetic flux bounded by a field line and the function $\chi = M \cos\theta/R^2$ is related to the distance along a field line. Note that $M \equiv B_0 R_0^3$ is the moment of the dipole magnet and (R, φ, θ) are spherical coordinates. Also note that the guiding center drift Hamiltonian is appropriate since energetic electrons produced in the experiment are non-relativistic.

When the particle motion is confined to the equatorial midplane of the magnetic field, $\rho_{\|} = \chi = 0$, $B = B(\psi)$, and the equations of motion are reduced to a particularly simple form. In general, particles will have a finite parallel velocity and will not be confined to the equatorial midplane. However, the precessional drift-frequency is only weakly dependent on pitch angle[1] and the results presented here would not be significantly altered by including parallel velocity.

The experimental observations described in the previous section indicate that the observed fluctuations can be modeled as a sum of traveling waves of the form:

$$\Phi(\varphi, t) = \frac{\Phi_0}{\sqrt{\mathscr{S}}}\sum_{m,l}^{N} a_{ml}\cos(m\varphi - \omega_l t + \varphi_l), \tag{2}$$

where $\mathscr{S} = \Sigma_{ml}|a_{ml}|^2$. The relative amplitudes, azimuthal mode numbers, frequencies, and phases are determined from the Fourier analysis of experimentally measured Langmuir probe signals. The waves observed in the experiment have a time-dependent frequency content, however, typically $t_{dh} d\log(a_{ml})/dt \ll 1$ and here we consider transport processes which occur on the time scale of several drift-periods.

For a single electrostatic wave the island half-width, $\Delta\psi$, at the resonant surface defined by $\omega_l - m\omega_{dh}(\mu, \psi_{lm}^r) = 0$, is given by: $\Delta\psi \simeq (2c\Phi_0\psi_{lm}^r/\omega_{dh})^{1/2}$. When multiple drift-resonant waves with sufficiently large amplitude are present, islands will overlap and lead to chaotic transport. The topological properties of particle trajectories can be determined by constructing the Poincaré surface of section which is formed by plotting (ψ, φ) at multiples of the mapping time. For a spectrum of waves, the mapping time is the least common multiple of the periods of the wave motion: $T_M = \mathrm{LCM}(T_l = 2\pi/\omega_l)$.[13] In practice, the frequen-

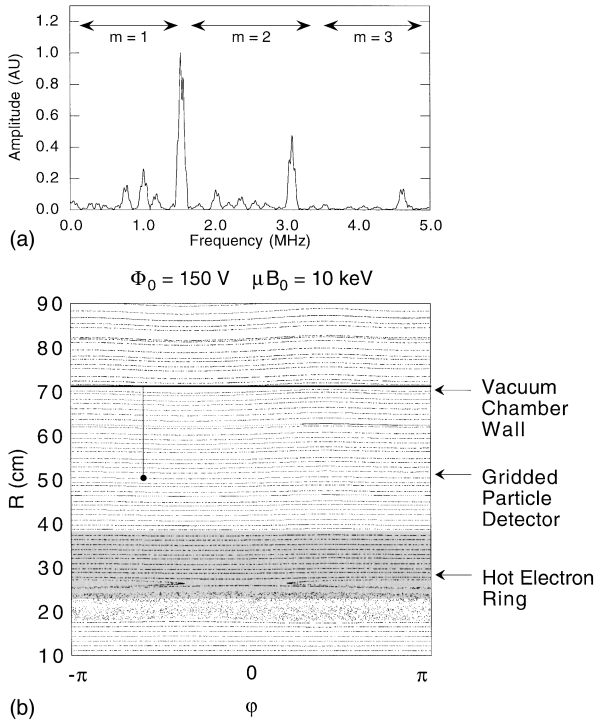

FIG. 3. A spectrum of waves taken from experimental measurements of fluctuations observed during the afterglow and a corresponding Poincaré surface of section. The chaos is localized to a thin, radially localized band near the hot electron ring and consistent with the absence of electron flux to the particle detector. The magnetic moment, μ, is chosen so that $\mu B_0 = 10$ keV; other parameters are $\Phi_0 = 150$ V, $N = 10$, and $T_M = 100$ μs. Note that the surface of section is plotted in (R, φ) coordinates.

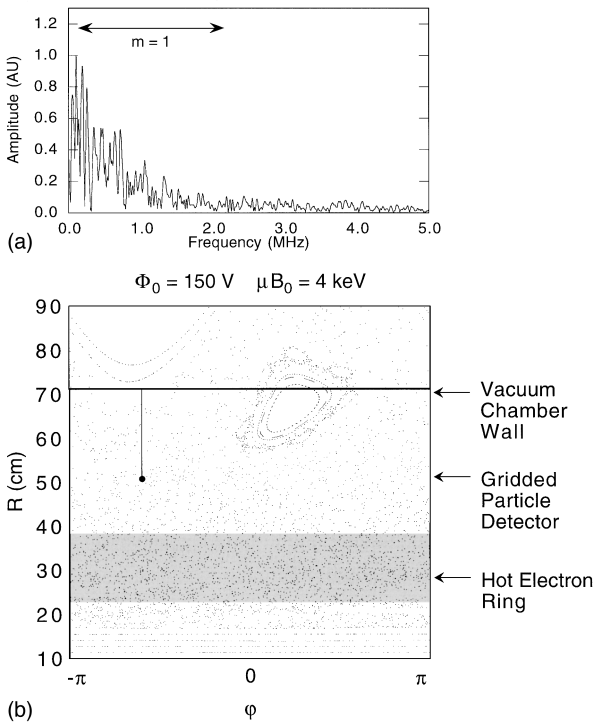

FIG. 4. A spectrum of waves taken from experimental measurements of fluctuations observed during the ECRH and a corresponding Poincaré surface of section. The fluctuations spectrum leads to chaos in ψ over the radial extent of the plasma. The magnetic moment, μ, is chosen so that $\mu B_0 = 4$ keV; other parameters are $\Phi_0 = 150$ V, $N = 10$, and $T_M = 100$ μs. Note that the surface of section is plotted in (R, φ) coordinates.

cies are rounded off to keep T_M from becoming too large. The equations of motion are integrated using the Gragg-Burlish-Stoer implementation of Richardson extrapolation.[14]

An example of a fluctuation spectrum used to model the electrostatic potential observed during the afterglow is shown in Fig. 3a. For electrons with energies above $\mu B_0 \approx 10$ keV this spectrum leads to resonant wave-particle interactions. However, as the Poincaré surface of section shown in Fig. 3b illustrates, the thin bands of chaos in ψ are limited to the proximity of the hot electron ring and do not extend out to the radial location of the gridded particle detector unless the amplitude of the potential fluctuations is very large.

A number of model fluctuation spectra have been constructed to model the potential fluctuations observed during the ECRH. For the wave spectrum shown in Fig. 4a, which is taken from the initial part of an instability burst, drift-resonances exist for electrons with energies between 1–10 keV (i.e., the ''warm'' electrons) from the center of the hot electron ring to the wall of the vacuum chamber. As shown in Fig. 4b, this spectrum of waves leads to chaos in ψ over the radial extent of the plasma. Examination of the phase space portraits indicates that when the wave amplitude is above $\Phi_0 \approx 75$ V, there are no encircling Kolmogorov-Arnol'd-Moser (KAM) surfaces[15] preventing global transport.

In order to demonstrate the relationship between the modulation of the current and the spectral content of the observed fluctuations, we have simulated the time-evolution of the flux of electrons to a small region of phase space which represents the particle detector. In the simulation, we randomly selected an ensemble of 5000 particle trajectories that are at the ''gridded particle detector'' at time $t = T$. Using spectral information from the experiment to construct the electrostatic potential in the form of Eq. (2), the equations of motion are integrated backwards in time from $t = T$ to $t = 0$ and the probability that the trajectory came from an assumed hot electron distribution, $F_h(\mu, \psi)$, is computed. This process is repeated in order to compute the current as a function of time.

The result of one such simulation is presented in Fig. 5 where it is compared with the corresponding energetic electron flux measurement from the experiment. Also shown in Fig. 5 is the Fourier transform of the simulated and measured electrostatic fluctuations as well as the Fourier transform of the simulated and measured energetic electron flux. The simulation successfully reproduces the frequency of the observed modulations as well as the relative amplitude. Since the phases of the measured waves and other profile parameters are unknown, the simulation cannot be expected to reproduce the temporal evolution of the particle flux exactly.

We have written a simple numerical simulation in order to compare the predictions of Hamiltonian and quasilinear descriptions of particle transport. In the code the simulated electron current is approximated by:

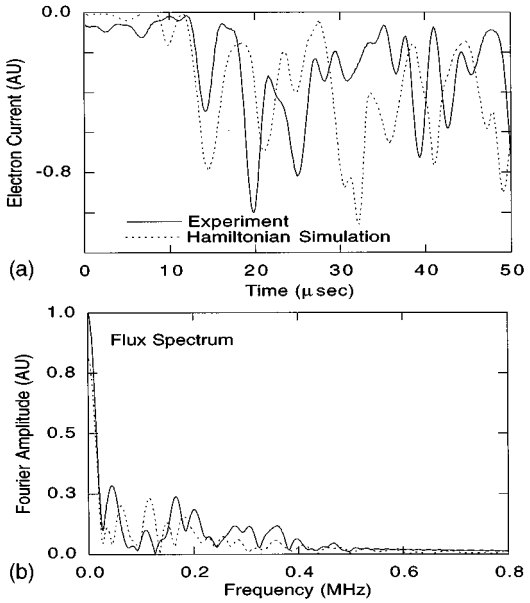

FIG. 5. A comparison of experiment and a simulation which reproduces the gross frequency and depth of the modulation. (a) Detected energetic electron flux, and (b) Fourier transform of the detected flux.

$$I(t)\approx eA\int d^3v\,vF_h(\mu,\psi_d,t)\sim eAn_0\alpha(\psi_d,t)\langle v\rangle, \qquad (3)$$

where $\langle v\rangle$ is the average velocity of particles reaching the detector. The function $\alpha(\psi,t)$ evolves according to a diffusion-like equation:

$$\frac{\partial\alpha}{\partial t}=\frac{\partial}{\partial\psi}\bar{D}_{\psi\psi}\frac{\partial\alpha}{\partial\psi}-\frac{\alpha}{t_L}\theta(\psi-\psi_d), \qquad (4)$$

where $\bar{D}_{\psi\psi}$ is the diffusion coefficient averaged over resonant velocities. The second term in Eq. (4) models particle losses due to the probe and $\theta(\psi-\psi_d)$ is the unit step function. The boundary conditions are set so that the solution goes to zero at the wall and the magnet casing.

The diffusion coefficient can be determined from integrating the equations of motion. In this case the diffusion coefficient is computed using the formula:

$$\bar{D}_{\psi\psi}=\frac{\langle(\psi(t)-\psi(0))^2\rangle}{2t} \qquad (5)$$

and the numerically determined value is used in the quasilinear simulation.

The result of a single run representative of the quasilinear simulation is shown in Fig. 6 where it is compared with the result from the corresponding Hamiltonian simulation. Significantly, the predictions of the quasilinear model do not reproduce the experimentally observed modulations and underestimate the maximum particle fluxes measured in the experiment.

V. SUMMARY AND DISCUSSION

This paper describes the experimental observation of wave-induced chaotic radial transport of energetic electrons in a laboratory terrella. In the experiment ECRH is used to create a localized population of energetic, magnetically trapped electrons. The trapped electrons excite quasiperiodic, drift-resonant fluctuations which are identified as the hot electron interchange instability. Increases in the flux of energetic particles to both the gridded particle detector situated near the equatorial midplane and the array of particle detectors located in the polar region are well correlated with the presence of the fluctuations. The radiation detected by the center photodiode also rises significantly during the instability bursts and is diminished between them. The measured particle fluxes are modulated at frequencies related to the precessional drift motion of the energetic electrons.

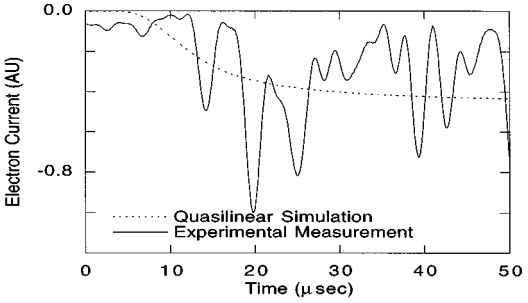

FIG. 6. A comparison of the experimental observation with the predictions of a quasilinear transport simulation. The predictions of the quasilinear model lack the large-scale modulations seen in the experimental data and underestimate that maximum observed particle fluxes.

This paper has also presented the detailed results of numerical simulations based on the guiding center drift equations which model transport processes observed in the experiment. Most significantly, the simulations confirm that the observed transport is the result of non-linear wave-particle interactions: transport is only observed when the wave-spectrum meets the conditions for global chaos; no transport is observed when the fluctuations lead to thin, radially localized bands of stochasticity.

The results of Hamiltonian simulations which explore the temporal details of the observed particle transport have also been presented. The relationship between chaotic mixing and the experimental measurements has been demonstrated by a simulation which models the flux of energetic particles to a small region of phase space. The simulation reproduces the frequency and depth of the observed modulation. In contrast, quasilinear models of transport do not reproduce the modulation of the particle flux and underestimate the maximum particle fluxes observed in the experiment.

The simulations described here model transport processes which occur on the time scale of several drift-periods. This time scale is short when compared with the evolution of an entire instability burst. Future research will focus on coupling transport simulations to a dispersion relation for the instability in order to investigate the self-consistent, nonlinear evolution of the plasma. This will allow us to address some of the unresolved questions related to the saturation of the instability and the chirping of the wave frequencies.

ACKNOWLEDGMENTS

This work has been supported by Air Force Office of Scientific Research Grant No. F4A-962093-10071, National Aeronautics and Space Administration Grant No. NAGW-3539, and National Science Foundation Grant No. ATM-91-11396.

[1]M. Schulz and L. J. Lanzerotti, *Particle Diffusion in the Radiation Belts*, No. 7 in *Physics and Chemistry in Space* (Springer-Verlag, New York, 1974).
[2]J. W. Dungey, Space Sci. Rev. **4**, 199 (1964).
[3]H. P. Warren and M. E. Mauel, Phys. Rev. Lett. **74**, 1351 (1995).
[4]H. P. Warren and M. E. Mauel, Phys. Plasmas **2**, 4185 (1995).
[5]H. P. Warren, A. Bhattacharjee, and M. E. Mauel, Geophys. Res. Lett. **19**, 941 (1992).
[6]M. Mauel, H. P. Warren, and A. Hasegawa, IEEE Trans. Plasma Sci. **PS-20**, 626 (1992).
[7]For example, R. A. Dandl, A. C. England, W. B. Ard, H. O. Eason, M. C. Becker, and G. M. Haas, Nuc. Fusion **4**, 344 (1964) or H. Ikegami, H. Ikezi, M. Hosokawa, S. Tanaka, and K. Takayama, Phys. Rev. Lett. **19**, 778 (1967).
[8]S. Hiroe, J. B. Wilgin, F. W. Baity, L. A. Berry, R. J. Colchin, W. A. Davis, A. M. El Nadi, G. R. Haste, D. L. Hillis, D. A. Spong, and T. Uckan, Phys. Fluids **27**, 1019 (1984).
[9]M. J. Gerver and B. G. Lane, Phys. Fluids **29**, 2214 (1986).
[10]N. A. Krall, Phys. Fluids **9**, 820 (1966).
[11]H. L. Berk, Phys. Fluids **19**, 1255 (1976).
[12]A. H. Boozer, Phys. Fluids **23**, 904 (1980).
[13]A. G. Kornienko, M. Y. Natenzon, R. Z. Sagdeev, and G. M. Zaslavsky, Phys. Lett. A **158**, 398 (1991).
[14]W. H. Press, B. P. Flannery, S. A. Teukolsky, and W. T. Vetterling, *Numerical Recipes: The Art of Scientific Computing* (Cambridge University Press, Cambridge, 1986).
[15]A. J. Lichtenberg and M. A. Lieberman, *Regular and Stochastic Motion*, No. 38 in *Applied Mathematical Sciences* (Springer-Verlag, New York, 1983).